A RADIANT-RESOLVED METEOROID MODEL

Andrew D. Taylor[1] & Neil McBride[2]

[1]Department of Physics and Mathematical Physics
University of Adelaide, SA 5005, Australia
Tel +61 8 8303 5996, Fax +61 8 8303 4384, Email ataylor@physics.adelaide.edu.au

[2]Unit for Space Sciences and Astrophysics
The Physics Laboratory, University of Kent, Canterbury, CT2 7NR, UK
Tel +44 (0)1227 823242, Fax +44 (0)1227 762616, Email N.McBride@ukc.ac.uk

ABSTRACT

We present a new meteoroid model which accounts for the variation with viewing direction of the numbers and speeds of meteoroids encountering the Earth. It is based on the ~20,000 meteor orbits obtained during the Harvard Radio Meteor Project synodic year survey. We define new radiant-specific velocity distributions for six broad radiant sources embedded in an isotropic flux. The relative mass distribution remains that determined by Grün *et al.* (1985), whilst the absolute flux levels are calibrated by running the model for the space face of NASA's Long Duration Exposure Facility (LDEF).

1. INTRODUCTION

The most widely used meteoroid flux model is currently that of Grün *et al.* (1985). This model offers *mean* fluxes to randomly orientated spacecraft surfaces and detectors *i.e.* it is essentially an isotropic model. However, the meteoroid environment is not isotropic (either in direction *or* speed). Additionally, spacecraft surfaces which maintain a specific geometry with respect to the Earth's motion through space (*e.g.* solar arrays) do not have a randomised exposure. This paper presents a meteoroid model, applied to spacecraft surface damage which accounts for anisotropies in the meteoroid environment.

2. METEOR RADIANTS AND VELOCITIES

The meteor radiant model developed by Brown and Jones (1995; Jones and Brown 1993) characterises the meteor radiant distribution in terms of six broad sources: Helion (HE), Antihelion (AH), North and South Toroidal (NT, ST), North and South Apex (NA, SA). The conversion, presented here, from the observed distribution, to one for meteoroids greater than a constant mass threshold, allows the relative numbers of meteoroids as a function of apparent radiant to be defined. The ~20,000 meteor orbits obtained during the Harvard Radio Meteor Project (HRMP) synodic year survey offers a statistically reliable database from which to determine meteoroid speed distributions as a function of radiant; mean values vary by a factor of ~6 across the sky. The relative mass distribution determined by Grün *et al.* (1985) is retained within this model and is used in preference to a single cumulative mass distribution exponent in converting to a constant mass threshold.

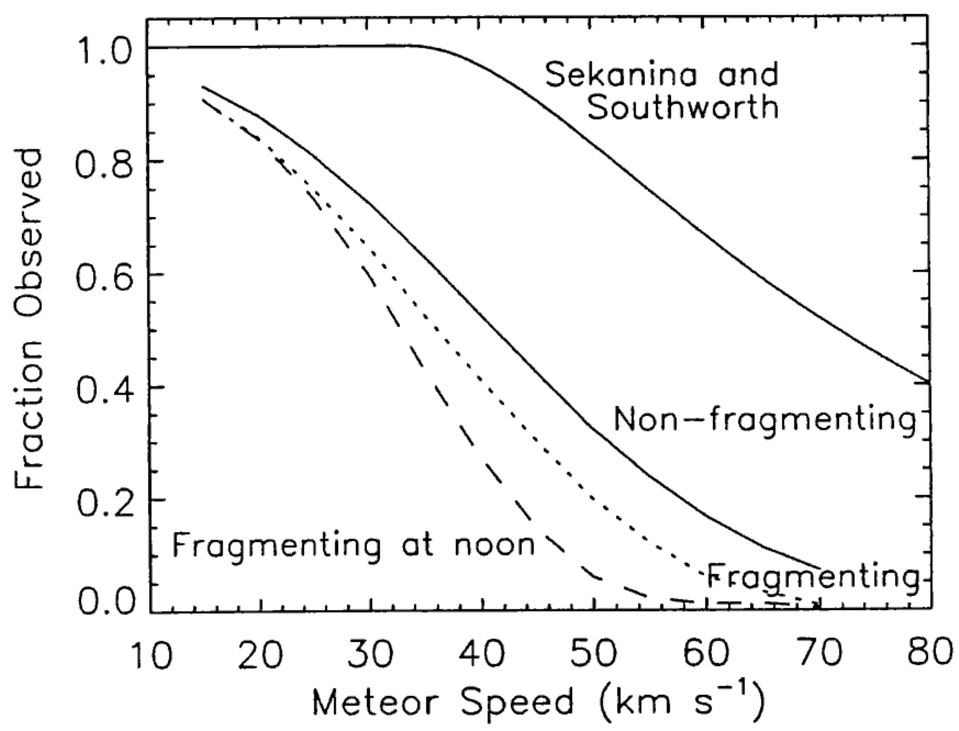

Figure 1: The figure shows the proportion of meteors at a given speed which go undetected due to the radio echo ceiling effect. The selection biases are due to meteor trial diffusion, and the onset of meteoroid fragmentation, as well as Faraday rotation effects. Southworth and Sekanina (1973) significantly underestimated the level of these effects.

The HRMP raw data are available from the IAU

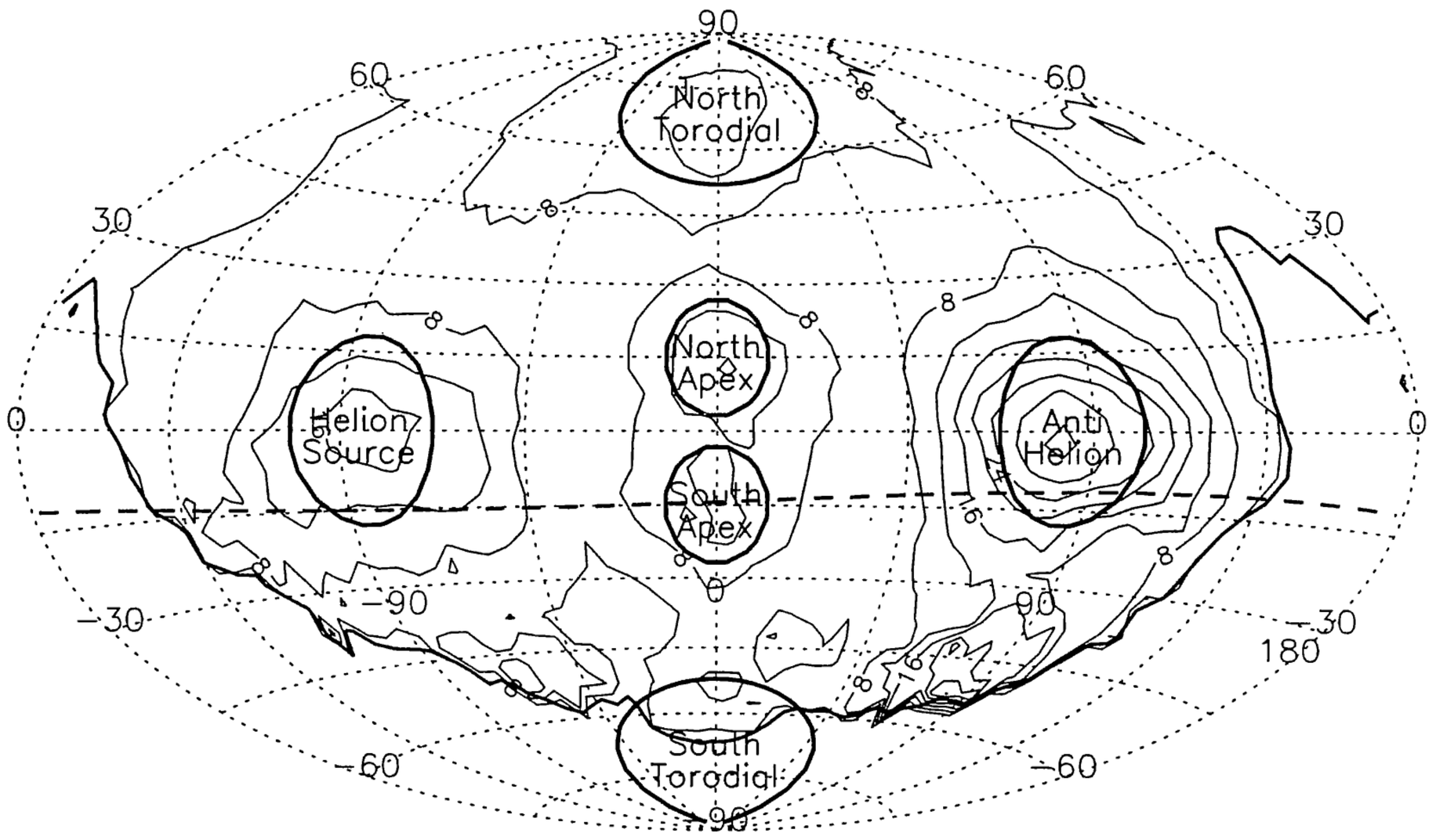

Figure 2: The radiant distribution of meteoroids with mass $m \geq 10^{-4}$ g encountering the Earth. The coordinate frame places the Earth's apex of motion at the center, the solar (Helion) direction at a longitude of $-90°$, and the north ecliptic pole at latitude $+90°$. The distribution is based on the Harvard Radio Meteor Project (HRMP) 1968–69 synodic year survey meteor orbit survey which has been corrected for selection effects associated with the radar, atmosphere and Earth's gravity. The heavy contour shows the region beyond which less than one meteor per (1/0.022) square degrees was detected, with correspondingly poor statistical reliability. Radiants south of the dashed line were observed for less than 10% of the time spent observing the celestial north pole (the most observed radiant). Contours south of both the 10% observing time and poor statistics (thick) lines are suppressed. The six radiant sources of the model are overlaid with the one sigma radii for each source marked.

Meteor Data Centre (Lindblad 1987; 1991). Elford and Hawkins (1964) calculated power distributions for various HRMP antenna configurations and went on to determine the relative observing time for each radiant, which was a function of declination when averaged over one day. By combining the observing schedule for the 1968–69 survey with these effective radar beam patterns a correction for station seeing has been made. Since no information has survived about the time at which receiver stations were active, the correction for station seeing remains uncertain by a factor of up to ∼50%. These uncertainties alter the width of the sources and may also be responsible for artificially enhancing the importance of the north toroidal source (at a constant mass threshold).

The rapid diffusion of meteoric ionization at high altitude introduces a radar echo ceiling. Fast meteors ionize at greater heights making this selection bias a function of speed. Elford (1997) summarised the various mechanisms which reduce the ability to detect meteors as a function of height, *i.e.*. finite initial radius of the trail, subsequent diffusion into the neutral atmosphere and the finite pulse rate of the radar. To determine a meteor's speed and hence be included the orbit catalogue, the trails have to remain detectable for a minimum time interval. Using a meteor ablation model similar to that of Love and Brownlee (1991) we generated a series of typical meteor ionization profiles as a function of speed (*cf* Elford *et al.* 1997). Convolving the height dependent detectability of a meteor with the sample ionization height profiles gives an estimate of the relative fraction of meteors missed when using the HRMP system. Fig. 1 compares the resulting bias-correction with that developed by Sekanina and Southworth (1975) which was used by them and Taylor (1995; 1997).

Elford and Taylor (1995) have shown that Faraday rotation is a significant effect for linearly-polarised back-scatter meteor radars. An allowance for this observational bias has been incorporated in the foregoing analysis and is presented as the 'noon' curve in Fig. 1. However the diurnal variation in ionospheric meteor heights coupled with the 1968–69 peak in solar activity makes this a very difficult observing bias to accommodate. The equivalent relative strengths for the HE and AH sources observed in the early 1960s, during sunspot miminum (Brown and Jones

1995) suggest we may have underestimated the necessary noon correction by a factor of ~50%.

The amount of ionization produced, and hence the radar detectability of a meteor at a given mass is a strong exponential function of the meteor's speed. Bronshten (1983) derived an expression for the total electron content of a meteor trail by combining the laboratory-measured ionization coefficients of atoms which typify the average composition of chondritic meteorites. Inserting this theoretical relation into the results of an empirical survey by Verniani (1973) the maximum electron line density has a mass–velocity dependence of $mv^{3.75}$. This is somewhat less than that employed by Taylor (1995). By combining this relation with the Grün *et al.* (1985) meteoroid mass distribution a conversion from the constant observation threshold to a constant mass threshold is made.

The relative numbers of meteoroids ($m \geq 10^{-4}$ g) are plotted in Fig. 2 as a function of the directions from which they approach the Earth. A correction for the flux enhancement due to the Earth's gravity has been incorporated. Incomplete coverage of the southern ecliptic hemisphere necessitates the assumption that the radiant distribution is symmetric about the ecliptic plane. The incomplete bias correction for the meteors observed around noon and during the afternoon principally affects meteors with radiants in the solar (helion) hemisphere. We assume symmetry about the apex-polar plane.

The speed distributions for all meteoroids within one sigma of a radiant source (w in Table 1) are plotted in Fig. 3. Gaussian fits to the have been adopted for the meteoroid model. A few low speed meteoroids have been partially ignored in fitting model distributions since they will be included in the isotropic source (see below). The radiant source pairs are assumed to both have the speed distributions of the best observed/bias-corrected partner.

The relative strengths of the various sources are based on the Brown and Jones (1995) analysis of two meteor rate surveys conducted during the 1960s. Within the uncertainties of their fits, these strengths are symmetrical about the ecliptic and apex-polar planes further supporting the above assumptions. These strengths have been converted to a constant mass threshold using the velocity distributions presented here (Fig. 3), the meteor detection criteria for the two surveys and a calculation of the fraction of meteors not observed (similar to that described above for the HRMP). The relative fraction of meteoroids at a constant mass threshold for each of the radiant sources are given as source strengths in Table 1.

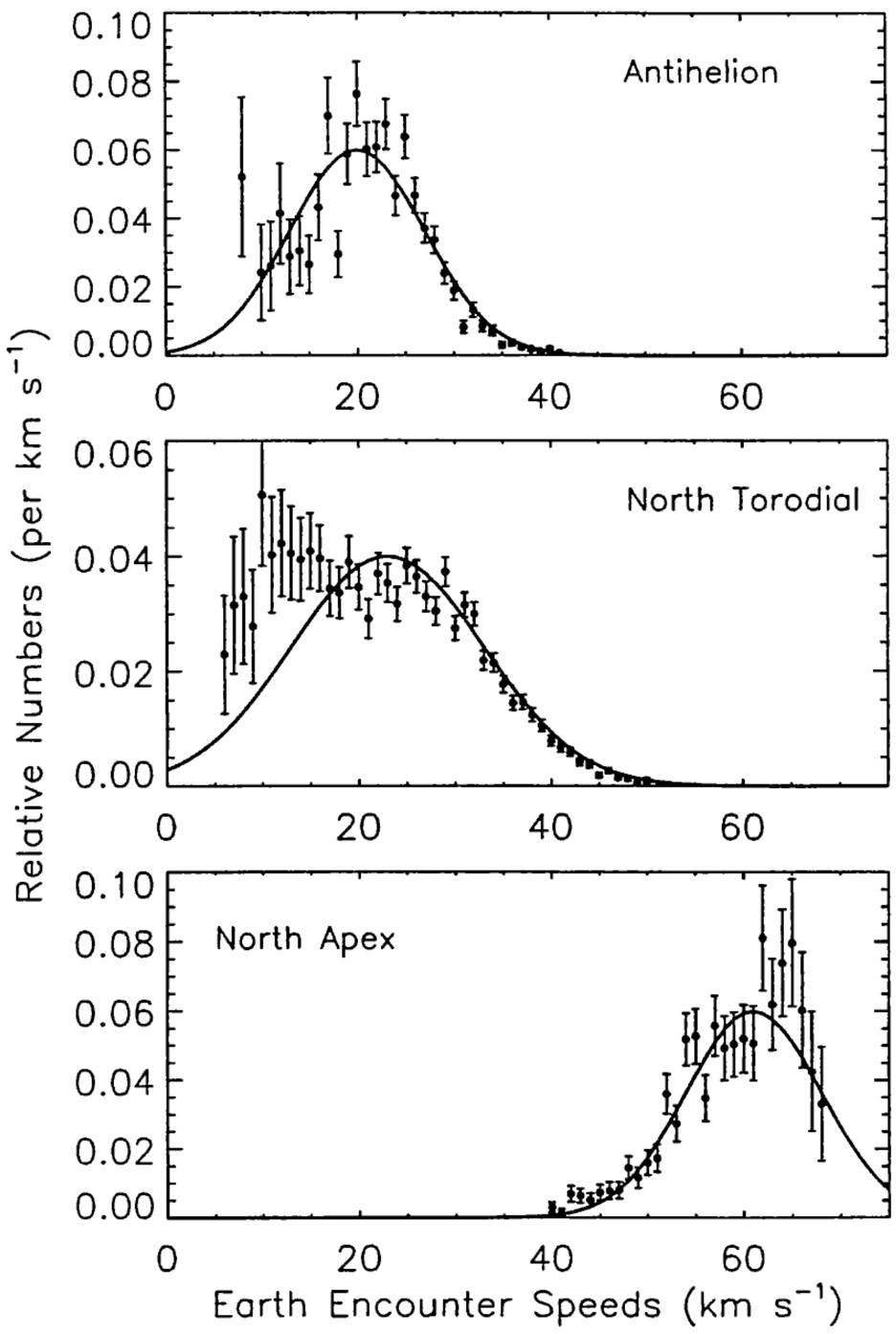

Figure 3: The speed distributions for all meteoroids with mass $m \geq 10^{-4}$ g, with radiants within one sigma of the source centres (*i.e.* within the enclosing circles of Fig. 3). The parameters for the Gaussian fits are in Table 1.

We assume that the broad background of meteoroid radiants can be characterised by an isotropic component within the model. To estimate the relative contribution made by this isotropic background the speed distribution from a representative sample of the sky (radiants in the antihelion hemisphere and north of the ecliptic) is compared with that which can be attributed to the various sources (Fig. 4). It should be emphasised that only the relative contribution of the isotropic component is adjusted in this process; the relative strengths of the radiant sources being fixed by independent meteor rate surveys. Fig. 5 compares the newly revised meteoroid speed distribution with previously published work. The improved analysis of the fraction of unobserved high-speed meteors is the principle difference from Taylor (1995). The rapid fall in numbers between 60 and 70 km s^{-1} is accounted for in this new radar echo-ceiling analysis. The slight revision of the velocity exponent used to determine the minimum detectable mass and the selection of a more uniformly sampled and bias-corrected section of the sky are

	λ	β	w	P	v	σ	S
ISO	—	—	—	1.0	9	5	0.42
HE	−85°	0	18°	21	20	7	0.20
AH	+85°	0	18°	21	20	7	0.20
NT	0	+70°	18°	21	23	10	0.05
ST	0	−70°	18°	21	23	10	0.05
NA	0	+15°	12°	47	61	6	0.04
SA	0	−15°	12°	47	61	6	0.04

Table 1: The model parameters. The radiant directions are given in terms of ecliptic longitude λ measured from the apex direction, and ecliptic latitude β. The radiant function f_ψ has a width (standard deviation) w and is scaled by the factor P. v ($\mathrm{km\,s^{-1}}$) is the velocity mean, and σ its standard deviation. S is the source strength.

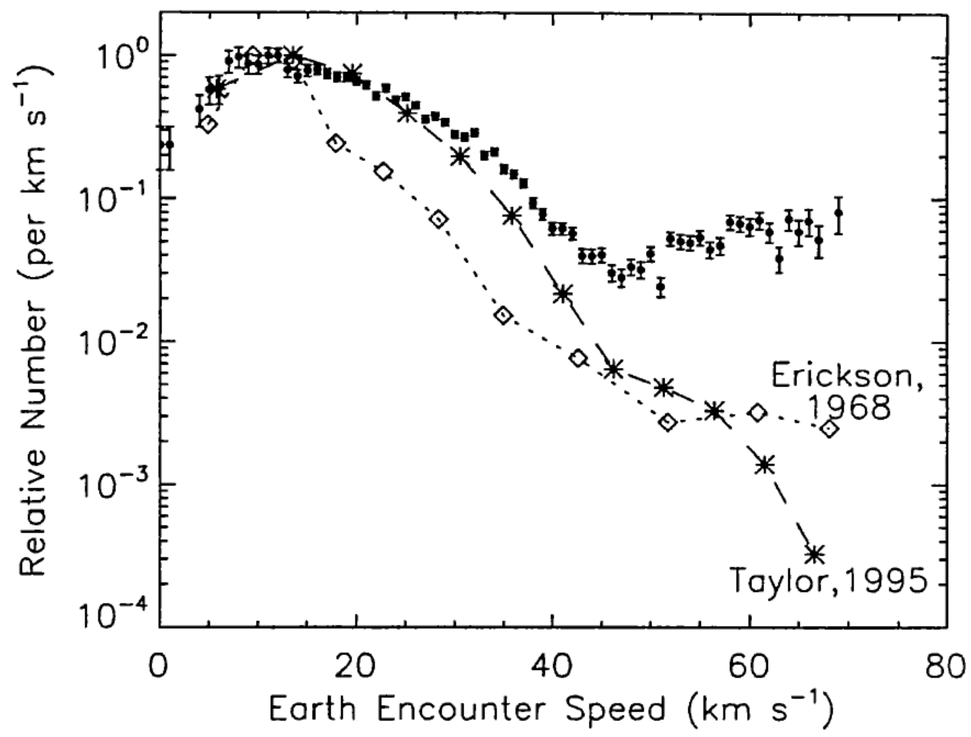

Figure 5: A comparison of the new HRMP meteoroid speed distribution with previously published data. Taylor (1995) identified a probable typographical error in the original analysis of the HRMP data by Sekanina and Southworth (1975) which had resulted in an underestimate of the relative importance of high speed meteoroids by a further factor of 100 below that shown here. Erickson (1968) used optical meteor data, corresponding to $m \geq 1$ g.

also important differences. Erickson (1968), using optical meteor data, deliberately excluded members of meteor showers and ensured that his 'randomly sampled' data set had a nearly uniform radiant distribution thereby significantly over-emphasising the isotropic source which is clearly evident in his published distribution. Most showers are members of the Helion/Antihelion and Apex sources and are therefore implicitly included in our model.

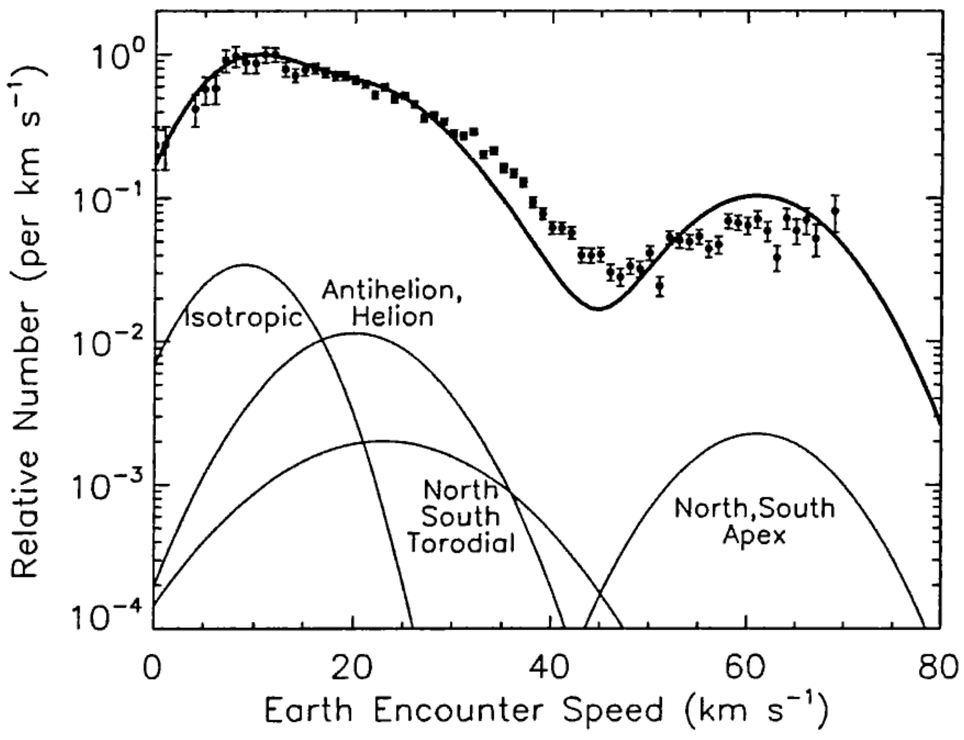

Figure 4: The speed distributions for all meteoroids with radiants north of the ecliptic and emanating from the antihelion hemisphere. The integrated area under the seven (isotropic and three pairs) component speed distributions has been normalised to one. The composite distribution and comparison with data have their peak values set to unity for clarity.

3. IMPLEMENTING THE MODEL

In the model, we use the mass distribution of Grün *et al.* (1985). At a given mass the absolute (differential) flux level as detected by a tumbling flat plate detector is F ($\mathrm{m^{-2}\ s^{-1}}$). The flux *intensity* ($\mathrm{m^{-2}\ s^{-1}\ sr^{-1}}$) is thus F/π. We then consider the flux of particles encountered by a moving flat plate detector by integrating the flux intensity over all viewing angles, particle mass, and particle speed. The total instantaneous flux contribution to the detector is then given by

$$F_m = \int_M \int_{v_\infty} \int_\phi \int_\theta \int_i f_i(\psi)\ \frac{F}{\pi}\ G\ S_i\ n(v_\infty) \cos A\ \frac{v_{\mathrm{rel}}}{v_E} \sin\theta\ di\ d\theta\ d\phi\ dv_\infty\ dm \quad (1)$$

where θ, ϕ are spherical polar coordinates with the spacecraft at the origin, v_E is the gravitationally enhanced meteoroid velocity given by $\sqrt{v_\infty^2 + v_{\mathrm{esc}}^2}$ (where v_{esc} is the escape velocity at the spacecraft altitude), v_{rel} is the relative velocity of the incoming meteoroid with respect to the spacecraft *i.e.* v_{rel}/v_E accounts for the spacecraft moving through the meteoroid environment, and the angle A is the instantaneous impact angle to the face (measured from the face normal). G is the gravitational flux enhancement given by $1+(v_{\mathrm{esc}}^2/v_\infty^2)$ (using a realistic minimum earth approach velocity $v_\infty > 1\,\mathrm{km\,s^{-1}}$). In numerical evaluation of Eq. 1, no instantaneous flux contribution is added if the meteoroid cannot impact the face (*i.e.* if $A > \pi/2$), or the spacecraft is shielded by the Earth. For source i, the overall weighting is performed via the strength factor S_i which essentially scales the *normalised* velocity distributions, which are themselves Gaussian. The distribution of meteoroids within radiant source i is defined by $f_i(\psi)$, the individual components of which vary with

the angle ψ between the direction of the source and the θ, ϕ. Aside from the isotropic source where $f(\psi)$ is set to unity everywhere, $f_i(\psi)$ is Gaussian with a standard deviation w:

$$f_i(\psi) = P_i \exp\left(-\frac{\psi^2}{2w^2}\right) \tag{2}$$

For an instantaneous di, $d\theta$, $d\phi$, dV_∞ and dM step, a damage equation may be used to obtain the ballistic limit F_{max} (maximum thickness of a foil which would be just-perforated) of a spacecraft detector *i.e.* each flux contribution is binned at the appropriate F_{max} value for the θ, ϕ, v_∞, M element. We use the penetration '1992c' equation of McDonnell & Sullivan (1992) where particle diameter d_p and F_{max} are in cm, and velocity V is in km s^{-1}.

$$\frac{F_{max}}{d_p} = 1.272\, d_p^{0.056}\, V^{0.806} \left(\frac{\rho_p \rho_{\rm Al}}{\rho_{\rm Fe}\rho_t}\right)^{0.476} \left(\frac{\sigma_{\rm Al}}{\sigma_t}\right)^{0.134} \tag{3}$$

The absolute differential flux levels (F) are defined by running the model for the space face of LDEF which, due to its gravity gradient stabilised orbit, had an essentially randomised exposure with respect to heliocentric space *i.e.* meteoroid anisotropies are averaged out over time (McBride *et al.* 1995) Further, very little orbital debris can impact the space face for geometric reasons and so the space face offers an excellent meteoroid calibration. The 'recalibration' of the flux levels over the Grün distribution is needed as the new velocity distribution has a higher mean velocity, so essentially shifting the mass (or F_{max}). As the effect is quite small, we shall simply adjust the absolute flux levels of Grün, such that the flux values F incorporated in the model are 75% that of Grün.

Fig. 6 shows the model applied to the space face of LDEF. Note that the north, south, east and west LDEF faces (which give the 5-face mean when combined with the space face) encounter orbital debris. The dominance of debris in LEO is clearly seen at the smaller sizes ($F_{max} < 30\mu$m). However, at the larger size regime ($F_{max} > 30\mu$m) meteoroids are dominant (McDonnell *et al.* 1997). This scenario in Fig. 6 is mirrored, almost identically, if running with only a purely isotropic meteoroid source due to LDEF's randomised exposure (see McBride & Taylor 1997).

We now consider the exposure to a spacecraft which does *not* have a randomised exposure with respect

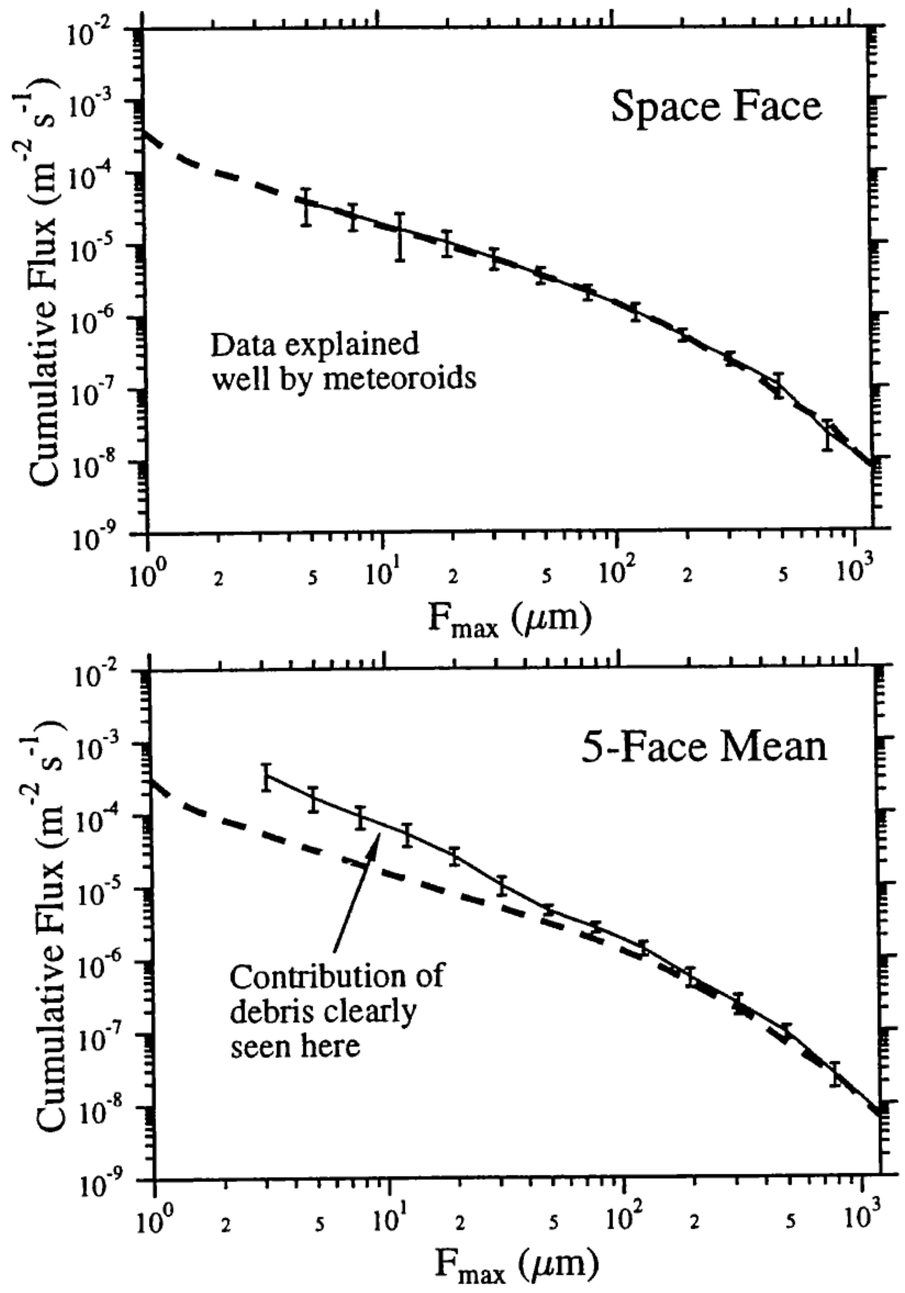

Figure 6: LDEF data is derived from a variety of sources *e.g.* the M&DSIG database (Zolensky *et al.* 1995; see McDonnell *et al.* 1997 for details) and is shown as a curve with error bars representing the typical spread in the data. The radiant-resolved model fits (dashed curves) are shown in comparison. Note the debris contribution at small sizes.

to the apex direction, in this case, a Sun-pointing spacecraft. We can consider the spacecraft as a cube with a Sun-pointing, apex-pointing and a north-pointing face. For simplicity we take the orbital plane to be parallel to the ecliptic plane which is a reasonable approximation for a typical precessing low Earth orbit. To demonstrate the possible effects of an anisotropic meteoroid source to an orientated spacecraft, we consider an extreme meteoroid model with only the apex sources (*i.e.* apex sources accounting for 100% of the particle flux). The results are shown in Fig. 7(a) for the Sun, apex and north faces of the orientated spacecraft, along with the 6-face mean obtained when running the nominal model with all sources with parameters given in Table 1. The range of flux levels is large. The north and Sun faces have different flux levels due to the slightly different Earth shielding scenarios (the north face has a constant shielding, and the Sun face varies between zero and total shielding). These effects are clearly important for highly collimated meteoroid sources

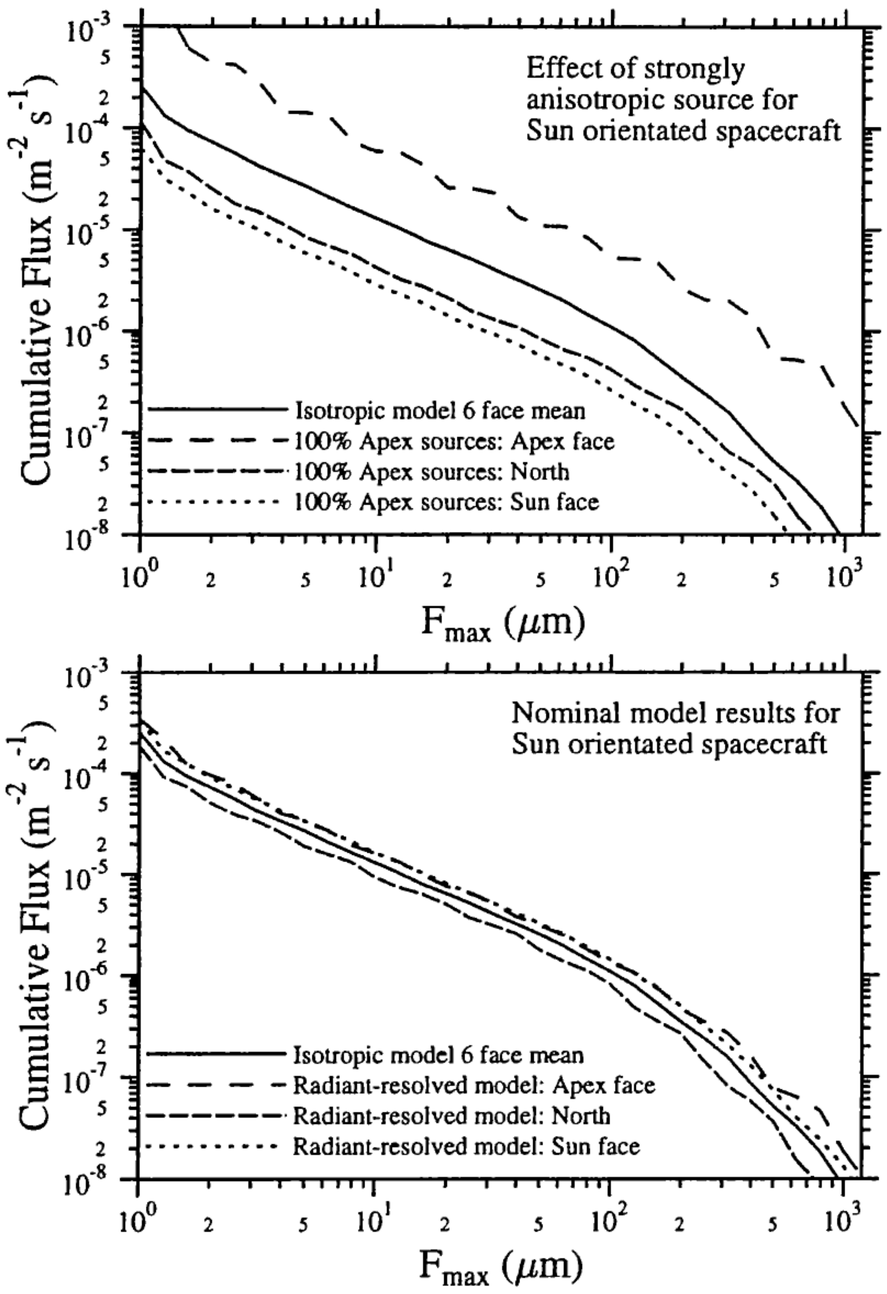

Figure 7: (a) Using only the apex sources (*i.e.* at 100% strength), we demonstrate the effect of an anisotropic meteoroid source on a Sun orientated spacecraft. The 'coarseness' of the apex curve is due to quantisation in the coding. (b) The nominal model (all sources). The anisotropy is 'diluted' although, specific collimated (or shielded) detectors may enhance exposure to a particular source.

(*e.g.* streams) or for collimated detectors (or semi-shielded spacecraft surfaces).

Fig. 7(b) shows the results for the nominal radiant-resolved model applied to the orientated spacecraft (*i.e.* all sources included). The difference between faces is less, due to the isotropic component and the virtually 'opposing' helion and anti-helion sources. Note however, that the Sun-pointing face exceeds the spacecraft mean level — this is directly applicable to solar array panels. The ratio of apex to anti-apex fluxes is ~ 2.

In the past, the role of fast meteoroids has been ignored or underestimated. However, fast meteoroids from the Earth apex direction could be very important for orientated or collimated detectors, especially for instruments which have a high velocity dependence such as plasma dust experiments.

4. REFERENCES

Bronshten, V.A., *Physics of meteoric phenomena*, Reidel, Dordrecht, 1983.

Brown, P., and Jones, J., A determination of the strengths of the sporadic radio-meteor sources, *Earth, Moon and Planets*, **68**, 223-245, 1995.

Elford, W.G., Scattering of radio waves from meteor trails, in *Interplanetary Dust*, eds. E. Grün, S.F. Dermott, H. Fechtig & B.Å.S. Gustafson, Univ. of Arizona Press, Tucson, in press, 1997.

Elford, W.G., Cervera, M.A. and Steel, D.I., Meteor velocities: A new look at an old problem, *Earth, Moon and Planets*, **68**, 257–266, 1995.

Elford, G.W. and Hawkins, G.S., Meteor echo rates and the flux of sporadic meteors, *Harvard Radio Meteor Project NASA Research Rep.*, no. 9, 1964.

Elford, W.G., Steel, D.I. and Taylor, A.D., Implications for meteoroid chemistry from the height distribution of radar meteors, *Adv. Space Res.*, in press, 1997.

Elford, W.G. and Taylor, A.D., Measurement of Faraday rotation of radar meteor echoes for the modelling of electron densities in the lower ionosphere, *J. Atmos. Terr. Phys.*, in press, 1997.

Erickson, J.E., Velocity distribution of sporadic photographic meteors, *J. Geophys. Res.*, **73**, 3721–3762, 1968.

Jones, J. and Brown, P., Sporadic meteor radiant distributions: Orbital survey results, *MNRAS*, **265**, 524–532, 1993.

Lindblad, B.A., in *Interplanetary Matter, Proc. 10th European Reg. Meeting of the IAU*, 2, eds Z. Ceplecha and P. Pecina, Prague, 201–204, 1987.

Lindblad, B.A., in *Origin and Evolution of Interplanetary Dust*, eds A.C. Levasseur-Regourd and H. Hasegawa, Kluwer Acad. Publishers, 311–314, 1991.

Love, S.G. and Brownlee, D.E., Heating and thermal transformation of micrometeoroids entering the Earth's atmosphere, *Icarus*, **89**, 26–43, 1991.

McBride, N., Taylor, A.D., Green, S.F. and McDonnell, J.A.M., Asymmetries in the natural meteoroid population as sampled by LDEF, *Planet. Space Sci.*, **43**, 757–764, 1995.

McBride, N., Taylor, E.A., The risk to satellite tethers from meteoroid and debris impacts, this volume, 1997.

McDonnell, J.A.M., Ratcliff, P.R., Green, S.F. & McBride, N., Micro-particle populations at LEO altitudes: recent spacecraft measurements, *Icarus*, in press, 1997.

Sekanina, Z. and Southworth, R.B., Physical and dynamical studies of meteors: Meteor-fragmentation and stream distribution studies, *NASA Contractor Report* **CR–2615**, Smithsonian Institution, Cambridge, MA, 1975.

Southworth, R.B. and Z.Ṡekanina. Physical and dynamical studies of meteors, *NASA Contractor Report* **CR 2316**, Smithsonian Institution, Cambridge, MA, 1973.

Taylor, A.D., The Harvard Radio Meteor Project meteor velocity distribution reappraised, *Icarus*, **116**, 154–158, 1995.

Taylor, A.D., Radiant distribution of meteoroids encountering the Earth, *Adv. Space Res.*, in press, 1997.